Advances in Science and Technology
Research Journal

Advances in Science and Technology Research Journal, 2025, 19(6), 167–180
https://doi.org/10.12913/22998624/203079
ISSN 2299-8624, License CC-BY 4.0

Received: 2025.02.20
Accepted: 2025.04.15
Published: 2025.05.01

Static analysis and topological optimization of photovoltaic panel support using recycled polymeric plastic

Javier Macedo[1], Jeanpiere Molina[1], Yuri Silva Vidal[1], Angel Mendoza[1],
José Canazas[1*], Christofer Diaz[1]

[1] Universidad Nacional de San Agustin de Arequipa, Arequipa 04000, Peru
* Corresponding author's e-mail: jcanazas@unsa.edu.pe

ABSTRACT

The rapid expansion of the photovoltaic solar system market has resulted in a significant increase in waste generated during installation, presenting a substantial environmental challenge. In response, the adoption of environmentally sustainable materials from various industries can play a crucial role in mitigating the effects of the ongoing climate crisis. This study explores the use of plastic polymer-based materials, including recycled and nanomaterials, for supporting photovoltaic solar panels. A preliminary structural design was subjected to static analysis, which facilitated the identification of a mechanically appropriate material for topological optimization. This optimization process led to a reduction in material usage and the proposal of three alternative support models. Among these, structures featuring hexagonal perforations demonstrated enhanced mechanical properties, achieving a mass reduction of up to 17.89%. The results of this study underscore the potential for incorporating recycled materials in the design of structural supports for photovoltaic solar panels, offering a viable pathway toward more sustainable photovoltaic infrastructure.

Keywords: support, solar panels, topological optimization, FEA.

INTRODUCTION

The global energy transition represents an imperative in the face of the contemporary climate crisis. According to statistics, fossil fuels dominate world energy consumption, constituting 83% of the energy matrix [1]. While these resources drove the Industrial Revolution and modern economic development, they harm the environment, as well as their limited nature and their role in global warming, have catalyzed the search for sustainable energy alternatives [1]. Significant challenges are now being faced in the transition to greener production. Increasingly stringent environmental regulations drive manufacturers to innovate in low-emission technologies, while consumer environmental awareness demands products with a lower carbon footprint [2, 3]. This is why a comprehensive transformation of production processes and corporate strategies of the productive sectors is required.

In recent years, renewable energies have emerged as viable options to address energy challenges. According to the International Energy Agency (IEA) [4], the global installed photovoltaic (PV) capacity reached a new record in 2022, with an increase of 26% over the previous year, reaching 1300 TWh. The solar panel structures on the market are mostly oriented to provide only mechanical support without considering the impact of the waste generated after their lifetime. It is estimated that global solar PV waste will reach 4–14% of total generation capacity by 2030 and increase to more than 80% by 2050 [5]. Currently, there are no standardized recycling methods or procedures in place, which complicates the implementation of environmentally efficient disposal practices. Solar panels are made from a variety of materials, some of which may pose potential risks to human health and the environment [6]. The main components of the panels are the frame, constructed of aluminum to provide structural support; that is, both the panel itself and the support structure are made of metallic materials [7], whose gradual deterioration raises environmental concerns related to the management of their waste, so alternating a different material in the components of photovoltaic solar systems allows for eco-friendly use of recycled products.

Floating solar photovoltaic technology first burst onto the global energy scene in 2007 [8] making a difference in renewable energy generation strategies, as they inserted plastics as part of the support structure, exactly in floats. Composite materials, particularly fiber-reinforced polymers (FRP), are experiencing an increasing integration in the maritime sector, thanks to their outstanding properties of corrosion resistance against marine environment [9] and their remarkable structural lightness [10, 11]. Significantly, FRPs have been preferred over traditional metals such as steel or aluminum in multiple floating production vessel (FPV) configurations [12], highlighting their innovative potential in marine engineering applications.

In recent years, more and more composite materials, in particular fiber-reinforced polymers (FRP), are being used in floating solar panels in the marine industry [12]. Polypropylene (PP), acrylonitrile butadiene styrene (ABS), polyethylene (PE), and polystyrene (PS) are the polymers that stand out even being recycled compared to other polymers [13]. To improve the capabilities of polymers, researchers have explored the creation of polymer matrix-reinforced composites by adding natural or synthetic fibers, as well as metals and ceramics [14]. Numerous researchers have examined how reinforcement with short or long fibers affects tensile [14] and compressive [15]. As part of the additives, we have multi-walled carbon nanotubes (MWCNTs) that exhibit optimal properties derived from their concentric molecular architecture; the synergy of interlayer interactions generates improved mechanical strength, overcoming the limitations of monolayer nanotubes. This unique structural configuration facilitates charge transfer between adjacent layers, enhancing their applicability in polymer composites requiring high mechanical strength.[16–18].

The application of recycled polymers in different types of structures has been studied in recent years. For example, Vicuña et al. [19] studied the use of recycled polypropylene and high-density polyethylene for the manufacture of geogrids used in the geotechnical sector. Experimental studies and finite element simulations were carried out to evaluate the structural strength of the geogrids. The results showed that the recycled high-density polyethylene has better mechanical properties and better performance. Additionally, chemical or biological tests are suggested according to the installation requirements of these geogrids. On the other hand, Azeez and Mohammed [20] performed modeling and structural analysis of sandwich panels from recycled plastic composites, reinforced with nanoparticles. The results showed that polycarbonate showed better performance over polypropylene and high-density polyethylene due to its high modulus of elasticity.

In the production market, when polymeric plastics are used, we have manufacturing methods such as additive manufacturing or 3D printing: however, this requires a large investment of time, we have the proposal of injection molding, this method is optimal for large-scale manufacturing, and for initiatives with long lead times [21]. Although it applies to components of various dimensions, this method has limitations in terms of design freedom. Elements manufactured using the injection molding process exhibit superior characteristics in terms of density, surface finish quality, dimensional accuracy, and reduced cycle times compared to the 3D printing manufacturing technique [22]. The injection molding manufacturing process is also distinguished by its reduced environmental impact, attributed to its high efficiency in both production and energy consumption. Unlike traditional 3D printing, which can involve significant use of energy and time, injection molding in polymers such as PLA optimizes these aspects by using less energy in its operational processes and requiring a smaller amount of raw material [23]. In this context, opportunities were identified to optimize processes, such as prioritizing suppliers with cleaner energy practices, implementing low-impact production technologies, and developing regulatory frameworks that encourage the systematic reduction of emissions in the manufacture of components for renewable energy [24, 25].

Additionally, structural optimization with the objective of achieving lighter designs has been a tool of considerable use in different industries such as automotive, biomedical, mining, etc. [26, 27]. Among the various studies of structural analysis and optimization of components, Zheng [28] performed a static and dynamic analysis study of a titanium alloy automotive structure and, with the objective of weight reduction, performed topological optimization studies, reducing in mass up to

13.76% without compromising the performance of the structure. On the other hand, Chidambaram et al. [29] developed a structural, modal, and thermal study of the two-wheeled electric vehicle battery enclosure using different metallic and thermoplastic materials. It was identified that a minimum clearance for insulation of 2.5 mm in the case of metallic enclosure and 10 mm in the case of thermoplastic material should be left. Then, Prabhuram et al. [30] performed a static analysis of different airless and conventional tire spoke structures considering various additive manufacturing polymers. From the results, it was identified that the diamond-type structure performed better than the honeycomb and triangular-type structures. From these studies, we can identify that the geometric conformation of the structure being evaluated is of utmost importance. In addition, the use of tools such as topological optimization or generative design in structures of flexible manufacturing materials allows the reduction of the amount of material to be used, maintaining the safety of the part to be designed.

This study addresses the application of recycled polymeric materials in supports for photovoltaic panels, evaluating their feasibility as a sustainable alternative to conventional materials. A comparative static analysis is performed between various polymeric plastics to determine their mechanical properties and structural suitability. The main objective is to develop an optimized support that, through topological optimization techniques applied to the strongest recycled polymer, manages to reduce the amount of material used without compromising structural integrity. This approach of double environmental benefit, use of recycled plastics and support for removable power generation, represents a significant contribution towards climate change mitigation.

METHODOLOGY

First, the characteristics of the solar panels that will be suitable for the support are described, and the support considers strength and operational stability parameters; then the materials to be evaluated will be defined through an analysis of their mechanical characteristics, including their resistance to static and dynamic loads, along with sustainability factors; finally, the details of the static analysis and topological optimization will be described using Solidworks software, where Von Mises and displacement simulations were performed to identify critical points, complemented with a topology study to optimize the design.

Solar panel support

The proposed approach involves several crucial steps: first, the development of parameters on the dimensions of the solar panels. Then, different parameters of polycrystalline, monocrystalline and thin film solar panels are conceptualized.

Figure 1a shows the support, which has been designed taking into account the dimensions specified in Table 1, particularly concerning the width of the solar panels. In addition, it is possible to identify the upper area, which is the surface intended to directly support the weight of the latter. This contact area is crucial, as it ensures the stability and safety of the system under the loads generated during operation. However, when installing the solar panels, the load of each panel will be distributed between two supports. In Figure 1(b), it can be seen that one of the supports is located at one end of the panel, while the other support is in contact with two solar panels, i.e., at the intersection of the two. The location of the intermediate support is arranged symmetrically, providing balanced support for both panels; this design ensures an even load distribution and contributes to the stability of the system during operation.

Regarding the fastening system of the panels, two specific solutions have been implemented to guarantee an optimal and safe installation. The first method employs a direct anchoring system using metal fasteners for interior fastening, i.e. between two panels as shown in Figure 2(a); as well as for exterior fastening in Figure 2(b), metal

Table 1. Solar panel dimensions

Type	Polycrystalline	Monocrystalline	Thin film
Power [W]	230–245	190–200	77.5–87.5
Height [mm]	1600–1700	1400–1300	1200
Width [mm]	900–1000	900–1000	600
Thickness [mm]	40–50	40–50	6–7

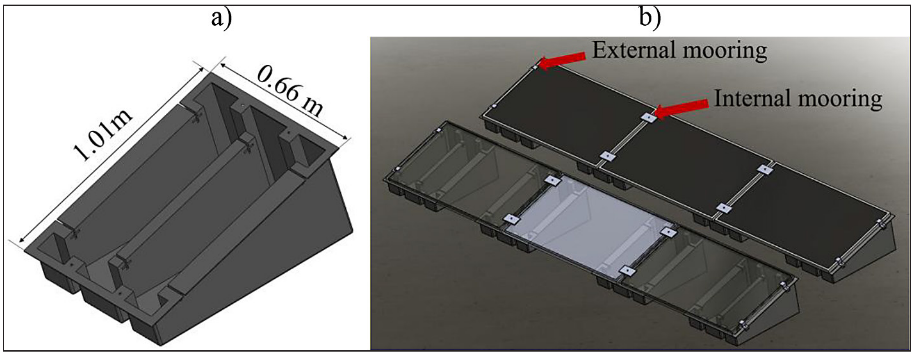

Figure 1. Dimensions and representation of the assembly with panels, (a) dimensions of the support, (b) arrangement of the solar panels supported on the support

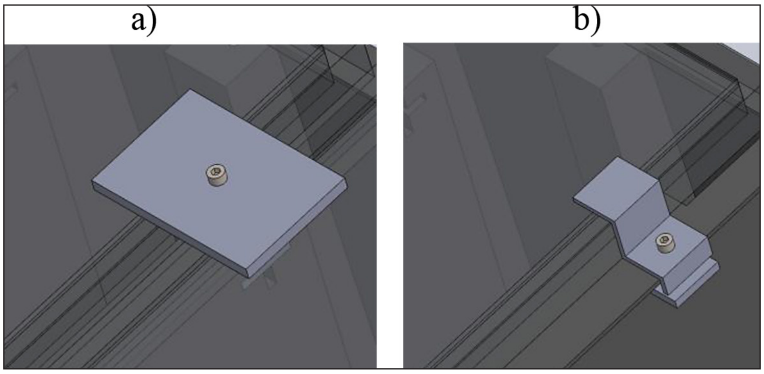

Figure 2. Mooring system for solar panels. (a) Interior mooring, (b) exterior mooring

fasteners with a different geometry are used, but like the first one, using DIN 912 M8 screws with allen head. To calculate the pressure exerted on the photovoltaic structure, the total area in contact was determined, by subtracting the area that does not have direct contact. It should be noted that for a solar panel, the intermediate support only makes contact with half the area of the support at the opposite end. For this reason, a multiplication factor of 1.5 is applied to adjust the calculation. Thus, the equation representing the area in contact for a panel is expressed as follows:

$$A_t = 1.5A_u - A_n \quad (1)$$

where: A_t is *the* total area in contact with the solar panel, A_u is the upper stand area and A_n is *the* area that is not in contact with the solar panel. $A_{total} = 1.5(239530.19) - 39765.2 = 0.319530m^2$

Table 2. Masses of panels and contact areas of panels with support structures

Type	Solar panel weight [kg]	Contact area [m^2]
Polycrystalline	13–20	3.1953 × 10^{-7}
Monocrystalline	13–24	3.1953 × 10^{-7}
Thin film	18–20	3.1953 × 10^{-7}

Table 2 shows the area and weight of each of the three types of solar panels. Considering the average weight of a 6-cell solar panel is 18 kg, the pressure exerted is 552.67 N/m2.

Wind loading occurs when moving air impacts a surface, causing dynamic energy to be converted into pressure. In the context of an urban area, values above the average wind speed were considered, as well as the inclination of the solar panel, which is 16°; in addition, the approximate height of 10-story buildings was taken into account, all to determine the factors that influence the wind pressure calculation. The pressure exerted on the panel surface translates into an effective force that must be considered in the design.

$$P = \frac{1}{2}\rho V_B^2 C_e C_f \quad (2)$$

where: P is the pressure of the wind, ρ is the density of the air, V_B is the wind speed, C_e is the combined coefficient for height and exposure and C_f is the coefficient of force or aerodynamic coefficient. Wind pressure with a speed of 41 *km/h* (11.4 *m/s*) $P_1 = 109.65375 N/m^2$, ind pressure with a speed of 90 *km/h* (25 *m/s*) $P_2 = 527.34375 N/m^2$

Consequently, the force exerted by the wind on the support will be:

$$F_1 = P \times A \tag{3}$$

$$F_1 = 109.65375 N/m^2 \times 0.319530 m^2 = 35.04 N$$

$$F_2 = 527.34375 N/m^2 \times 0.319530 m^2 = 168.5021 N$$

Material

Six polymers were used as support structure material for the solar panel, for the respective simulation of each of them, the mechanical properties such as elastic modulus, Poisson's ratio, tensile strength, and density were identified; with each of them, the von Mises and displacement simulation will be performed. The incorporation of multi-walled carbon nanotubes (MWCNTs) in PP matrices represents an innovative strategy to significantly improve the mechanical properties of polymeric materials, even after recycling processes [31]. This technique allows increasing parameters such as tensile strength, elastic modulus, and impact resistance through the homogeneous dispersion of nanotubes in the polymeric structure, generating composites with superior mechanical characteristics than those without any type of additive Nanotubes exhibit superior mechanical and electrical properties thanks to their interlayer interactions. This unique feature enables significant improvement in structural integrity and performance, positioning them as cutting-edge materials for applications demanding high strength and optimization of physical properties in various technological industries [17], maintaining their performance even after recycling. Atila Bata et al. developed a study where, the mechanical performance of recycled polypropylene (PP REC) after incorporation of multi-walled carbon nanotubes (MWCNT) was examined; Young's modulus of the base polymer experienced a significant increase from 1662 MPa to 1874 MPa upon addition of 1% w/w MWCNT, representing a substantial 13% improvement in its mechanical properties. This increase in the elastic modulus demonstrates the potential of carbon nanotubes to reinforce the polymer structure, Table 3 shows the properties of the polymers used for the simulation.

Static analysis

The simulation was carried out using the Simulation module in SolidWorks 2023, specifically using the static analysis study. This was selected for its efficiency in handling structural problems. The discretization of the domain was performed using elements where the meshing used was based on the combined curvature, which provides adequate accuracy in the calculation of stresses and deformations. Table 4 gives more details of the mesh parameters, such as Jacobian points for high-quality mesh, total number of elements, total number of nodes, etc.

The von Mises stress can be obtained thanks to the principal stresses according to the following expression:

$$\sigma_{VonMises} = \sqrt{\frac{(\sigma_1+\sigma_2)^2+(\sigma_2+\sigma_3)^2+(\sigma_1+\sigma_3)^2}{2}} \tag{4}$$

The von Mises criterion of failure posits that material yield begins when the equivalent voltage reaches the stress limit, formally expressed as:

$$\sigma_{\text{vonMises}} \geq \sigma_{\text{limit}} \tag{5}$$

where: creep strength is conventionally adopted as a critical parameter, although the software allows the use of maximum tensile strength or the establishment of a custom limit value, the safety factor is quantified by the relationship:

$$\textit{Factor of safety}\ (\text{FOS}) = \sigma_{llimit}/\sigma_{vonMises} \tag{6}$$

In the case of pure shear stress, where only $\sigma_{12} = \sigma_{21} \neq 0$, for others $\sigma_{12} = 0$, the critical stress according to von Mises's criterion is reduced to:

Table 3. Properties of polymers

Type	Elastic modulus [N/m²]	Poisson's ratio	Yield stress [N/m²]	Density [kg/m³]
PP homopolymer	1.79×10^9	0.4003	3.84×10^{-7}	933
PP REC	1.66×10^9	0.3803	3.83×10^{-7}	933
PP/MWCNT REC	1.85×10^9	0.3403	3.92×10^{-7}	933
PE high density	1.11×10^9	0.41	2.21×10^{-7}	952
ABS	2.00×10^9	0.394	2.21×10^{-7}	1020
Rigid PVC	2.4×10^9	0.3825	4.07×10^{-7}	1300

Table 4. Mesh parameters

Type of mesh	Solid mesh
Mesh stitch used	Mesh-based on the combined curvature
Jacobian stitches for high-quality mesh	16 points
Maximum element size [mm]	10.904
Minimum element size [mm]	0.57246
Mesh quality	High-order quadratic elements
Total number of nodes	361133
Total number of elements	180732
Maximum aspect ratio	65.101
Percentage of elements with aspect ratio < 3	97.1
Percentage of elements with aspect ratio > 10	0.0913

$$\sigma_{12}máx = \sigma_{yield} / \sqrt{3} = 0.5777\ (\sigma_{yield}) \tag{7}$$

This relationship shows that, at the beginning of plasticization, the maximum permissible shear stress under pure shear conditions is approximately $\sqrt{3}$ times lower than the yield stress observed in the case of simple tension.

SIMP method for topology optimization

Among the different existing approaches, the solid isotropic material with penalization (SIMP) approach, developed by researchers Bendsoe and Kikuchi in 1988, and later by Rozvany and Zhou in 1992, stands out. This methodology analyzes how to distribute the material based on several factors: applied forces, boundary conditions, manufacturing constraints, and desired performance. Bendsoe explained in 1989 that the optimization process must establish whether it is necessary to place material at each location in the available space [32]. The conventional method divides the total area into a finite element mesh, wherein each design domain, the material distribution is individual, and each element is assigned a binary value:

$$\rho_{(e)} = 1 \tag{8}$$

$$\rho_{(e)} = 0 \tag{9}$$

The penalty factor p reduces the influence of intermediate densities and guides the optimization towards a clear binary solution: completely solid elements ($\rho_{(e)} = 1$) or empty elements ($\rho_{(e)} = 0$). Experimentally, a value of p = 3 has been determined to be optimal. [32]. According to the SIMP approach, the global stiffness is adjusted according to:

$$K_{SIMP(\rho)} = \sum_{e=1}^{N}[\rho_{\min} + (1-\rho_{\min})\rho_e^p] \tag{10}$$

where: K_e is the element's stiffness matrix, ρ_{min}. is the minimum relative density, ρ_e is the relative density of the element, p is the penalty factor, and N is the number of elements in the design domain.

The main objective is to achieve maximum overall stiffness by minimizing the overall compliance, C, with a specific reduction in mass. Through an iterative process, the algorithm optimizes the element densities to minimize the overall compliance, which is equivalent to maximizing the stiffness of the structure.

$$\min C(\{\rho\}) = \sum_{e=1}^{N}(\rho_e)^p[\mathrm{u}_e]^T[\mathrm{K}_e][\mathrm{u}_e] \tag{11}$$

where: $[u_e]$ is the nodal displacement vector of element e, $[K_e]$ is the stiffness of element e, and the vector $\{\rho\}$ contains the relative densities of the elements ρ_e. In each cycle of the optimization process, three fundamental conditions need to be satisfied: reaching the set mass target, maintaining the overall strength-stiffness balance, and meeting the set functional requirements:

$$\sum_{e=1}^{N}\{v_e\}^T \rho_e \le M_{target} \tag{12}$$

where: the volume of the component is represented as v_e, while $M_{\{target\}}$ indicates the mass to be achieved in the optimization.

$$[\mathrm{K}\{\rho\}]\{\mathrm{u}\} = \{\mathrm{F}\} \tag{13}$$

where: the matrix $[K\{\rho\}]$ represents the global stiffness affected by the vector of relative densities, while $\{u\}$ indicates the displacement vector, and $\{f\}$ represents the external forces.

$$\theta(\{\rho\},\{\mathrm{u}\})_1 \leq \theta_1^*, \theta(\{\rho\},\{\mathrm{u}\})_2 \leq \leq \theta_2^*, \theta(\{\rho\},\{\mathrm{u}\})_3 \leq \theta_3^*, ... \quad (14)$$

The above formula contains design response constraints, such as limits on stresses, displacements, eigenfrequencies, etc. In each iteration, the optimization algorithm performs a sensitivity study to determine how changes in material concentration affect the goal of achieving maximum stiffness. During this sensitivity study, components that have a low material concentration lose relevance in the structure and are eliminated in subsequent cycles. Assessing the sensitivity of each component in isolation, without taking into account how they are connected, can result in material discontinuities and separate sections of the main structure [32]. This phenomenon is known as a checkerboard pattern. To minimize this situation, a filtering method is applied that considers a radius of influence and averages the sensitivities of each component within its impact zone. The iterative process continues until the changes in the objective function stabilize and the established convergence criteria are satisfied.

RESULTS

A static analysis was carried out in Solidworks Professional to evaluate the mechanical performance of different candidate materials in a support structure for solar panels. The study included static simulations that provided maximum values of von Mises stress and displacement under standard loading conditions.

Equivalent stress

A support model is evaluated, using six different materials in Solidworks: homopolymer PP, PP REC, PP/MWCNT, High-Density PE, ABS, and rigid PVC, to determine the equivalent stress according to the von Mises criterion. Figure 3 compares the results of the simulations showing the von Mises stress distribution for the proposed polymeric materials in the solar panel support. Finite element analysis revealed significant differences in the von Mises stress distribution among the different polymeric materials evaluated for photovoltaic support. The homopolymer PP exhibited a maximum stress of 1.19 × 10^5 N/m², while its recycled counterpart (PP REC) showed a maximum value of 1.20 × 10^5 N/m². The incorporation of carbon nanotubes in the recycled PP (PP/MWCNT REC) resulted in a value of 1.20 × 10^5 N/m². HDPE presented a maximum stress of 1.19 × 10^5 N/m², being the lowest among all the materials evaluated, followed by homopolymer PP and ABS with 1.20 × 10^5 N/m². Rigid PVC showed the second-highest maximum stress of 1.21 × 10^4 N/m². The stress distribution, represented by a chromatic scale from 0 to 1.00 × 10^5 N/m², indicates that the stress concentrations are mainly located in the geometric transition zones

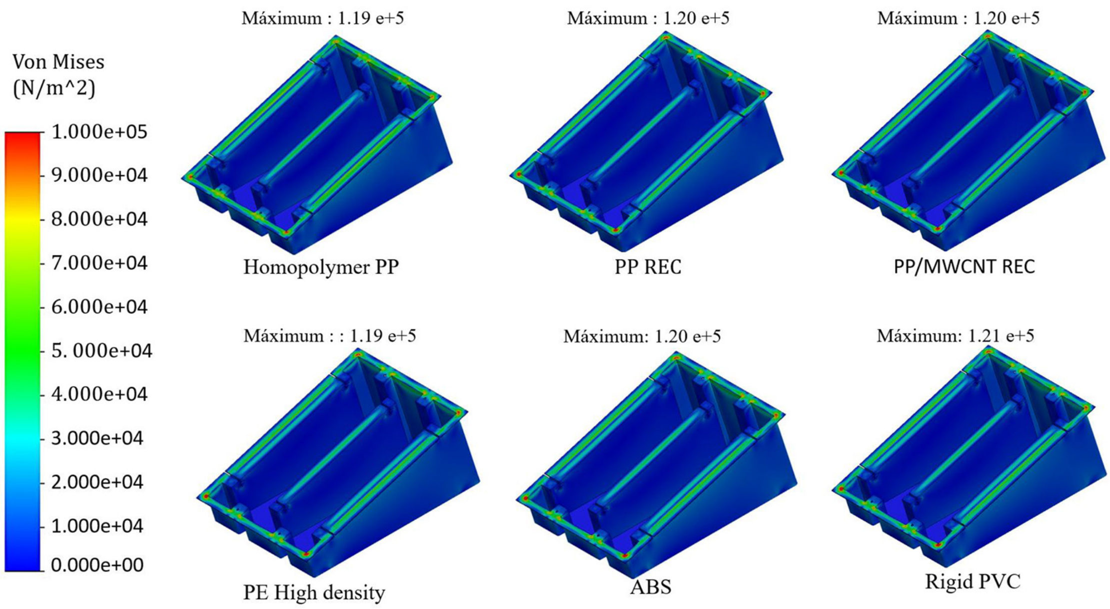

Figure 3. Comparison of the equivalent von Mises stress of the support using various polymers

of the support, while the regions in blue denote areas of lower mechanical stress. These results indicate that HDPE and homopolymer PP offer the best performance for this specific application, considering the stress distribution and maximum values observed.

Regarding the design of the polymeric support for solar panels, Figure 3 shows the critical points with higher von Mises stresses, which correspond to the fastening elements and supports subjected to higher loads. This highlights the importance of avoiding decreasing the thickness of the side walls supporting the PV panel, this is already complemented by topological optimization.

Displacement

The study examines the support, evaluating its mechanical behavior under six different polymer compositions, the main objective being to quantify the resulting maximum deformations. Figure 4 illustrates the displacement distribution obtained for each material variant analyzed.

From the displacement analyses (URES) performed in the simulation of different polymeric materials for solar panel supports, significant results were obtained that allowed the evaluation of their structural feasibility. The comparative analysis of the displacement in supports manufactured with different polymeric materials reveals distinctive mechanical behaviors that are crucial for their structural application. The results show a clear influence of the material composition on the deformation resistance, where PP/MWCNT REC exhibits a maximum displacement of 2.10×10^{-2} mm, representing an improvement over homopolymer PP (2.04×10^{-2} mm) and PP REC (2.25×10^{-2} mm). This optimization in performance can be attributed to the effective incorporation of carbon nanotubes in the polymeric matrix, which act as nanometer reinforcement improving the structural stiffness of the recycled material. In the evaluation of alternative materials, rigid PVC demonstrates superior performance with the smallest maximum displacement (1.76×10^{-2} mm), followed by ABS (1.86×10^{-2} mm), while high-density PE exhibits the largest displacement (3.39×10^{-2} mm). These results suggest that, while the incorporation of MWCNT significantly improves the mechanical properties of recycled PP, rigid PVC emerges as the most effective option for applications requiring maximum resistance to deformation. The distribution of displacements, visualized by the color scale, indicates more uniform deformation patterns in the better-performing materials, suggesting a more efficient distribution of applied loads.

Table 5 shows the comparison for the equivalent Von-Mises stress, as well as for the comparison of the support displacement using the 6 polymers already mentioned; the mesh convergence study carried out on the different polymeric materials revealed a remarkable stability in the stress and deformation results. Three element sizes (0.05, 0.57 and 1.06 mm) were analyzed, the results showed that the maximum von Mises stress and displacement remained practically constant (for the mesh that has a minimum distance

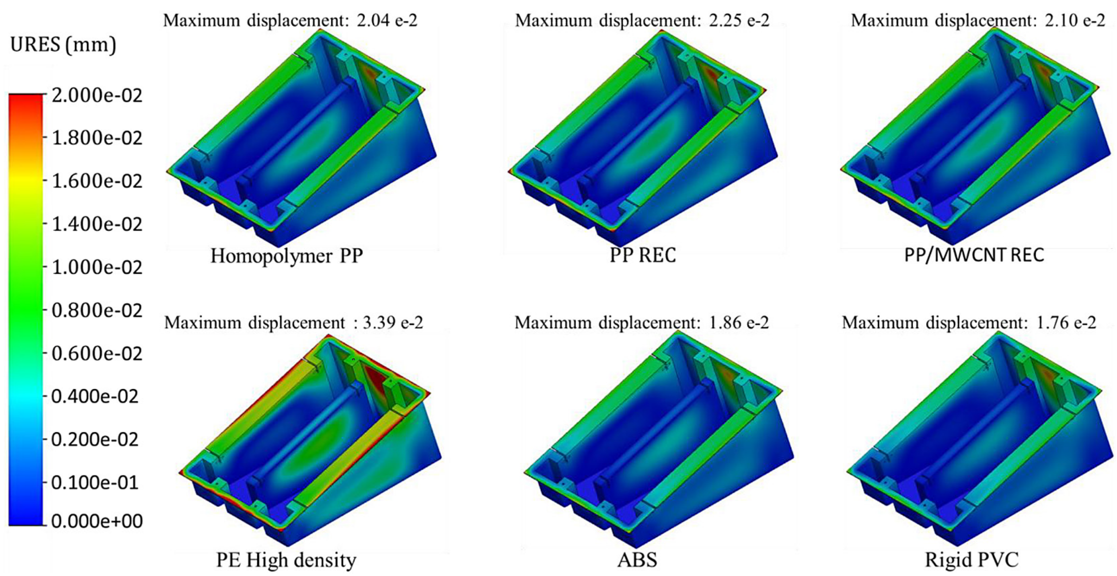

Figure 4. Comparison of support displacement using various polymers

Table 5. Simulation results

Type	Von mises max [N/m²]			Max displacement [mm]		
Minimum item size (mm)	0.05	0.57	1.06	0.05	0.57	1.06
PP homopolymer	1.19×10^5	1.19×10^5	1.19×10^5	2.04×10^{-2}	2.04×10^{-2}	2.01×10^{-2}
PP REC	1.20×10^5	1.20×10^5	1.21×10^5	2.25×10^{-2}	2.25×10^{-2}	2.21×10^{-2}
PP/MWCNT REC	1.20×10^5	1.20×10^5	1.19×10^5	2.10×10^{-2}	2.10×10^{-2}	2.08×10^{-2}
PE high density	1.19×10^5	1.19×10^5	1.19×10^5	3.39×10^{-2}	3.39×10^{-2}	3.37×10^{-2}
ABS	1.20×10^5	1.20×10^5	1.20×10^5	1.86×10^{-2}	1.86×10^{-2}	1.85×10^{-2}
Rigid PVC	1.21×10^5	1.21×10^5	1.23×10^5	1.76×10^{-2}	1.76×10^{-2}	1.76×10^{-2}

Note: for different wind speeds, the simulation was performed and the results are presented in Table 6.

Table 6. Simulation results for different wind speeds

Type	Von mises max [N/m²]		Max displacement [mm]	
Wind speed	11.4 m/s	25 m/s	11.4 m/s	25 m/s
PP homopolymer	1.19×10^5	2.11×10^5	2.04×10^{-2}	3.66×10^{-2}
PP REC	1.20×10^5	2.12×10^5	2.25×10^{-2}	4.03×10^{-2}
PP/MWCNT REC	1.20×10^5	2.12×10^5	2.10×10^{-2}	3.77×10^{-2}
PE High density	1.19×10^5	2.15×10^5	3.39×10^{-2}	6.07×10^{-2}
ABS	1.20×10^5	2.12×10^5	1.86×10^{-2}	3.30×10^{-2}
Rigid PVC	1.21×10^5	2.13×10^5	1.76×10^{-2}	2.78×10^{-2}

between elements of 0.05 and 0.57), which indicates that 0.57 mm is an intermediate size that generates reliable and accurate results for the structural analysis of these polymers. It is observed that the PP/MWCNT REC has a behavior similar to the average, of course, it is not better than the pure polymers, but the additive allows to improve these properties. That is why PP/MWCNT REC will be used as a material for topological optimization.

Topological optimization

This process uses the SIMP method implemented through algorithms, in the specific case of solar panel supports. The geometric configurations resulting from the simulation are presented in Figure 5, from the areas that Solidworks recommends us to keep and eliminate.

The topological optimization process was carried out by minimizing the objective function C and implementing critical parameters such as the penalty factor p = 3 and a filter radius = 1.2. Figure 6 shows a significant and controlled reduction of the structural mass over 76 iterations, where a steep decrease is observed in the first 8 iterations, followed by a gradual stabilization phase. The topological optimization considers multiple constraints such as allowable displacement limits, Figure 7 shows that over 76 iterations the constraint was met.

Figure 8 shows the three geometries resulting from the topological optimization show different material distribution patterns. The geometry in Figure 8a has horizontal grooves of varying length, distributed non-uniformly along the surface, creating trajectories for load distribution.

The configuration in Figure 8b exhibits vertical slots aligned in regular patterns, suggesting a more systematic distribution of stresses throughout the structure. Finally, the geometry in Figure

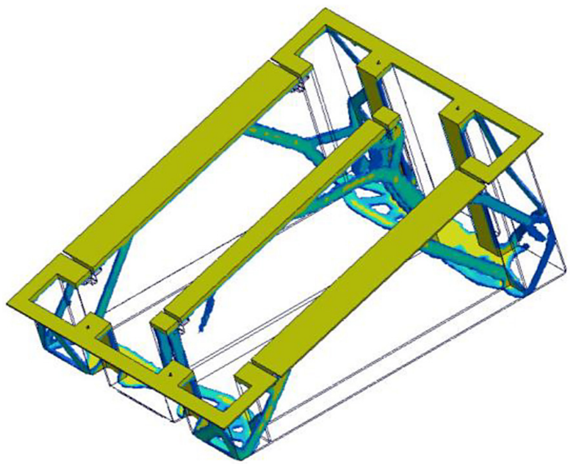

Figure 5. Topology optimization results

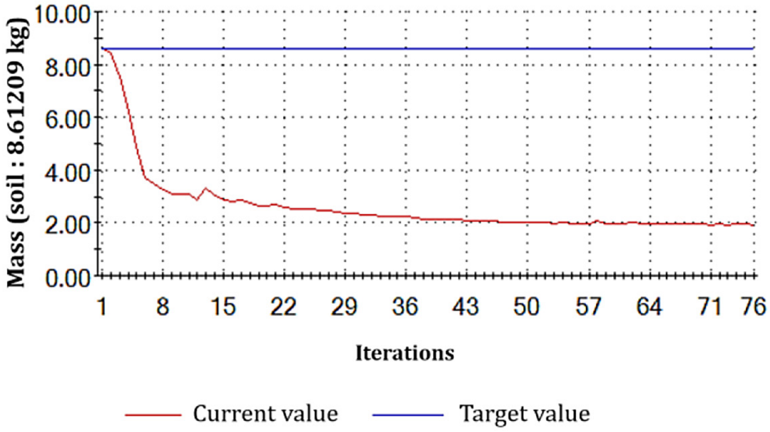

Figure 6. Objective function convergence during topology optimization to minimize mass

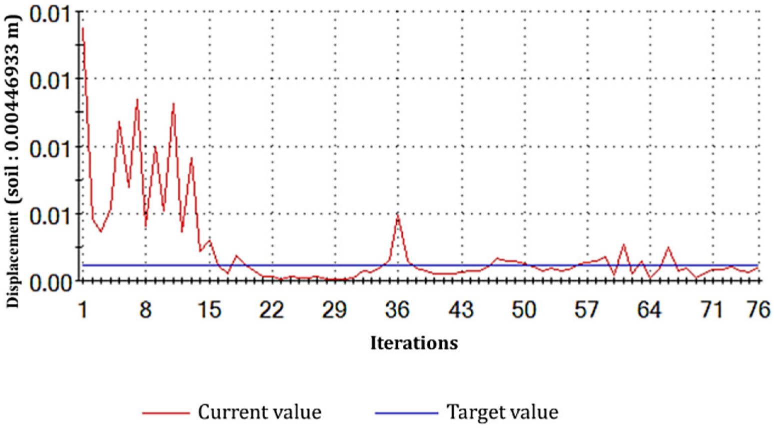

Figure 7. Convergence of the objective function during topology optimization with the displacement constraint

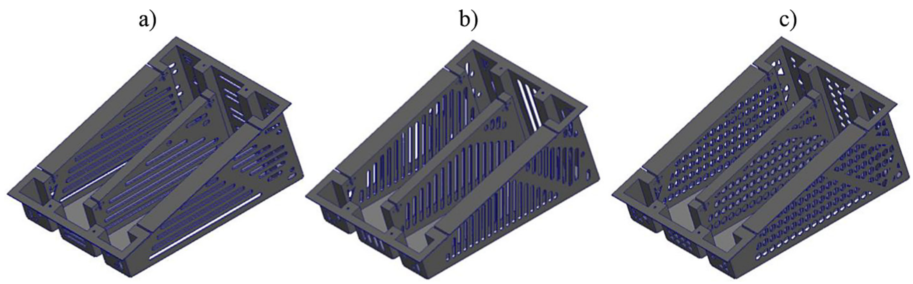

Figure 8. New geometries after topology optimization simulation; (a) geometry with horizontal grooves, (b) geometry with vertical grooves, (c) geometry with hexagonal holes

8(c) implements a uniformly distributed hexagonal hole pattern, mimicking natural structures such as honeycombs, which typically provide an optimal strength-to-weight ratio. Each design represents a unique solution to the trade-off between reducing material and maintaining structural integrity. Complementary finite element analyses are recorded in Figures 9 and 10, while dimensional and volumetric variations of the optimized design are quantitatively detailed in Table 4. Von Mises stress analysis reveals distinctive patterns among the three geometric configurations studied. The geometry with horizontal slots shows the highest maximum stress of 2.27e+5 N/m², with stress concentration zones visible in the central areas. The configuration with vertical slots shows an intermediate maximum stress of 1.69e+5 N/m², suggesting a better stress distribution. The geometry with hexagonal holes shows the best behavior with the lowest maximum stress

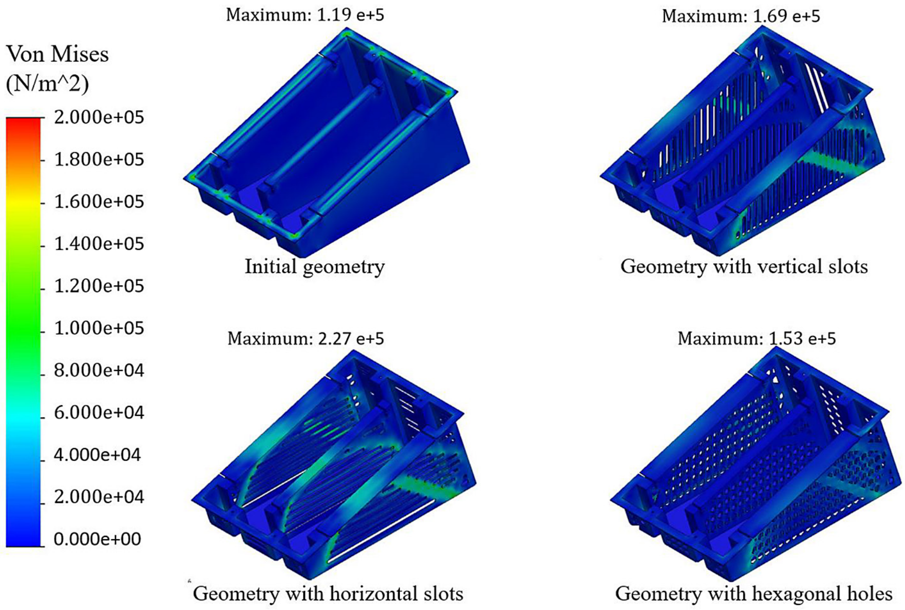

Figure 9. Comparison of equivalent von Mises stress after topology optimization

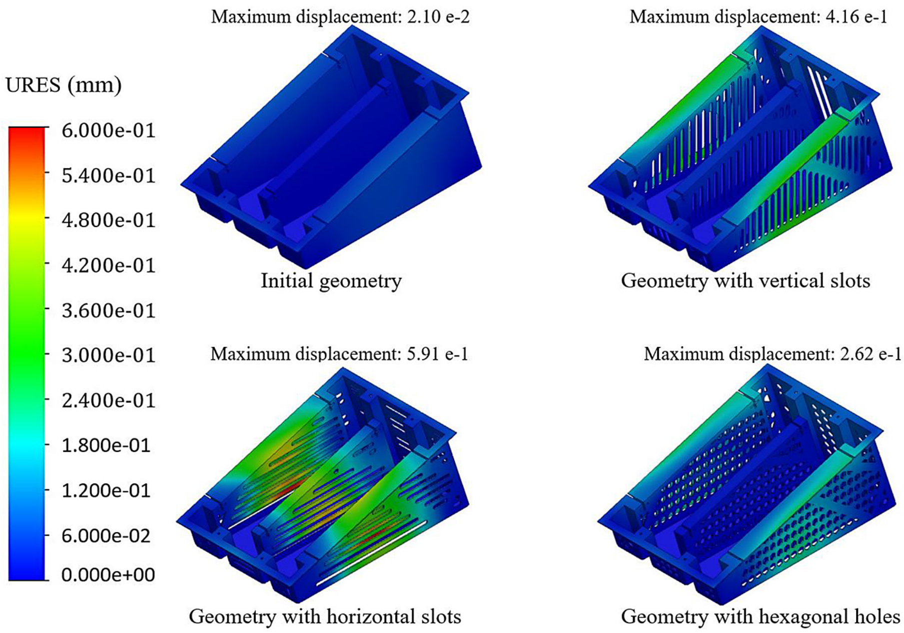

Figure 10. Comparison of displacement after topology optimization

of 1.53e+5 N/m² and a more uniform stress distribution, as evidenced by the predominance of blue color throughout the structure. These results indicate that the hexagonal configuration is not only more efficient in terms of stress distribution but also minimizes stress concentration points.

The results of the displacement analysis performed on three different configurations of a support-type structure reveal interesting patterns in terms of their mechanical behavior. The geometry with horizontal grooves exhibited the largest maximum displacement of 5.91e-1 mm, showing zones of deformation concentration more pronounced in the central areas, evidenced by the green regions indicating displacements of approximately 0.24–0.42 mm. On the other hand, the configuration with vertical grooves presented a smaller maximum displacement of 4.16e-1 mm, suggesting a better distribution of loads along the structure. The stress distribution in this case shows a more uniform pattern, with fewer zones of high displacement concentration. Finally, the

Table 7. Variation in volume and mass of the final model

Feature	Unit	Horizontal slot	Vertical slot	Hexagonal holes
Initial volume	[m^3]	0.01383	0.01383	0.01383
Final volume	[m^3]	0.01099	0.01090	0.01135
Initial mass	[kg]	12.91	12.91	12.91
Final Mass (optimized)	[kg]	10.26	10.17	10.60
Displacement of the new design	[m]	0.000591	0.000416	0.000262
Average displacement increment	[m]	0.00057	0.000395	0.000241
Relationship between final displacement and initial displacement	[%]	2810	1980	1250
Increase of the final von Mises stress with respect to the initial design	[Pa]	1.08×10^5	4.91×10^4	3.28×10^4
Ratio between initial and ultimate von Mises stresses	[%]	190	141	127

geometry with hexagonal holes showed the best behavior in terms of structural stiffness, with a significantly lower maximum displacement of 2.62e-1 mm. This hexagonal design appears to optimize load distribution throughout the entire structure, as evidenced by the predominance of blue color in the model, indicating minimal displacements over most of the surface. The color scale, ranging from 0 to 0.5 mm, clearly shows how the hexagonal configuration keeps most of the structure in displacement ranges of less than 0.15 mm (Table 7).

CONCLUSIONS

In the present work, the static analysis of support for photovoltaic panels was carried out, with different polymeric materials, including one recycled and another with MWCNT, to then reduce material through topological optimization, resulting in 3 new designs with a lower mass, these 3 designs, thanks to the finite element analysis were compared to determine the most optimal design.

The results of the simulation made on the support show that among the materials analyzed, HDPE shows the highest maximum displacement, while rigid PVC shows the lowest displacement. As for the Von Mises stress, rigid PVC exhibits the highest value, suggesting that this material experiences higher internal stress under the simulated loading conditions for the solar panel support. However, the variations in the results of the simulations with virgin polymers and PP-MWCNT REC are not much, thanks to the additive, this polymer was used as the material for the topological optimization.

Topological optimization performed in the three different configurations reveals significant results in terms of structural efficiency and mechanical performance. The three designs started from an identical initial volume and an initial mass of 13.83 kg, but showed different behaviors after optimization. The configuration with hexagonal holes proved to be the most efficient, with a final volume (0.01135 m^3) and mass (10.60 kg), since it exhibited the lowest average displacement increase (0.241 mm) and the lowest final/initial displacement ratio. In addition, this configuration exhibited the lowest voltage increase (3.28×10^4 Pa). On the contrary, the horizontal groove configuration, although it achieved a volume reduction similar to the vertical one (approximately 0.01099 m^3), showed the highest values in displacement increment (0.00057 m) and tension (1.08×10^5 Pa). The results suggest that hexagonal geometry might be the most favorable choice for applications where strain minimization is critical, likely due to the more uniform distribution of stress provided by this geometric pattern. The progression in the reduction of the maximum displacement from configuration (a) to (c) demonstrates how the proper selection of the geometric pattern can significantly influence the mechanical behavior of the structure, offering important implications for the design and optimization of similar components in engineering applications. However, for future research, it might be interesting to conduct a study of cost and mass, i.e. the improvement of transport and assembly costs.

Acknowledgments

This research has been carried out thanks to the support of the Universidad Nacional de San Agustin de Arequipa.

REFERENCES

1. Holechek JL, Geli HME, Sawalhah MN, Valdez R. A global assessment: can renewable energy replace fossil fuels by 2050? Sustainability. MDPI AG 2022; 14: 4792. http://dx.doi.org/10.3390/SU14084792
2. Jiang F, Huang W, Yang J, Duan H. Retailer involvement in eco-conscious consumer-oriented carbon footprint reduction. European Journal of Operational Research. 2025; 322: 795–811. http://dx.doi.org/10.1016/j.ejor.2024.10.030
3. Rumsa M, John M, Biswas W. Global steel decarbonization roadmaps: Near-zero by 2050. Environmental Impact Assessment Review 2025; 112: 107807. http://dx.doi.org/10.1016/j.eiar.2025.107807
4. International Energy Agency (IEA). Tracking Clean Energy Progress 2023, Assessing critical energy technologies for global clean energy transitions [Internet]. París: International Energy Agency; 2023. [cited 2024 Dec 19] Available from: https://www.iea.org/reports/tracking-clean-energy-progress-2023
5. Chowdhury MdS, Rahman KS, Chowdhury T, Nuthammachot N, Techato K, Akhtaruzzaman Md, et al. An overview of solar photovoltaic panels' end-of-life material recycling. Energy Strategy Reviews 2020; 27: 100431. http://dx.doi.org/10.1016/j.esr.2019.100431
6. Tammaro M, Salluzzo A, Rimauro J, Schiavo S, Manzo S. Experimental investigation to evaluate the potential environmental hazards of photovoltaic panels. Journal of Hazardous Materials 2016; 306: 395–405. http://dx.doi.org/10.1016/j.jhazmat.2015.12.018
7. Maghraby YR, Ibrahim AH, Tayel A, Mohamed El-Said Azzazy H, Shoeib T. Towards sustainability via recycling solar photovoltaic Panels. Solar Energy 2025; 285: 113085. http://dx.doi.org/10.1016/j.solener.2024.113085
8. Trapani K, Redón Santafé M. A review of floating photovoltaic installations: 2007–2013. Progress in Photovoltaics: Research and Applications. Wiley; 2014; 23: 524–32. http://dx.doi.org/10.1002/pip.2466
9. Rubino F, Nisticò A, Tucci F, Carlone P. Marine application of fiber reinforced composites: A review. Journal of Marine Science and Engineering. MDPI AG; 2020; 8: 26. http://dx.doi.org/10.3390/jmse8010026
10. Yousuf H, Khokhar MQ, Zahid MA, Kim J, Kim Y, Cho EC, et al. A Review on floating photovoltaic technology (FPVT). Current Photovoltaic Research 2020 Sep 30; 8(3): 67–78. https://doi.org/10.21218/CPR.2020.8.3.067
11. Koondhar MA, Albasha L, Mahariq I, Graba BB, Touti E. Reviewing floating photovoltaic (FPV) technology for solar energy generation. Energy Strategy Reviews 2024; 54: 101449. http://dx.doi.org/10.1016/j.esr.2024.101449
12. Claus R, López M. Key issues in the design of floating photovoltaic structures for the marine environment. Renewable and Sustainable Energy Reviews 2022; 164. http://dx.doi.org/10.1016/j.rser.2022.112502
13. Yousaf A, Al Rashid A, Polat R, Koç M. Potential and challenges of recycled polymer plastics and natural waste materials for additive manufacturing. Sustainable Materials and Technologies 2024; 41: e01103. http://dx.doi.org/10.1016/j.susmat.2024.e01103
14. Liu Z, Lei Q, Xing S. Mechanical characteristics of wood, ceramic, metal and carbon fiber-based PLA composites fabricated by FDM. Journal of Materials Research and Technology 2019; 8: 3741–51. http://dx.doi.org/10.1016/j.jmrt.2019.06.034
15. Ajay Kumar M, Khan MS, Mishra SB. Effect of fused deposition machine parameters on tensile strength of printed carbon fiber reinforced PLA thermoplastics. Materials Today: Proceedings 2020; 27: 1505–10. http://dx.doi.org/10.1016/j.matpr.2020.03.033
16. Jagadeesh P, Puttegowda M, Thyavihalli Girijappa YG, Rangappa SM, Siengchin S. Effect of natural filler materials on fiber reinforced hybrid polymer composites: An Overview. Journal of Natural Fiberr 2020; 19: 4132–47. http://dx.doi.org/10.1080/15440478.2020.1854145
17. Patti A, Barretta R, Marotti de Sciarra F, Mensitieri G, Menna C, Russo P. Flexural properties of multi-wall carbon nanotube/polypropylene composites: Experimental investigation and nonlocal modeling. Composite Structures 2015; 131: 282–9. http://dx.doi.org/10.1016/j.compstruct.2015.05.002
18. Zidan HM, Abdelrazek EM, Abdelghany AM, Tarabiah AE. Characterization and some physical studies of PVA/PVP filled with MWCNTs. Journal of Materials Research and Technology 2019; 8: 904–13. http://dx.doi.org/10.1016/j.jmrt.2018.04.023
19. Vicuña L, Jaramillo-Fierro X, Cuenca PE, Godoy-Paucar B, Inga-Lafebre JD, Chavez Torres JL, et al. Evaluation of the effectiveness of geogrids manufactured from recycled plastics for slope stabilization—A case study. Polymers. MDPI AG 2024; 16: 1151. http://dx.doi.org/10.3390/polym16081151
20. Azeez A, Mohammed S. Solidworks simulation of mechanical properties of recycled plastics/nanocomposite faces sandwich panels. ARO-The Scientific Journal of Koya University 2018; 6: 65–70. http://dx.doi.org/10.14500/aro.10394
21. Islam MA, Mobarak MH, Rimon MIH, Al Mahmud MZ, Ghosh J, Ahmed MMS, et al. Additive manufacturing in polymer research: Advances, synthesis, and applications. Polymer Testing 2024; 132: 108364. http://dx.doi.org/10.1016/j.polymertesting.2024.108364
22. Akbar I, El Hadrouz M, El Mansori M, Tarfaoui M.

Investigation of thermo-mechanical shape memory signatures of 3D printed and Injection molded polymers. CIRP Journal of Manufacturing Science and Technology 2023; 41:277–91. http://dx.doi.org/10.1016/j.cirpj.2022.12.011

23. Alex Y, Divakaran NC, Pattanayak I, Lakshyajit B, Ajay PV, Mohanty S. Comprehensive study of PLA material extrusion 3D printing optimization and its comparison with PLA injection molding through life cycle assessment. Sustainable Materials and Technologies 2025; 496, 43: 01222. http://dx.doi.org/10.1016/j.susmat.2024.e01222
24. Zhang H, Lang C, Zhang R. Life cycle carbon footprint analysis of suitcase production: Impact of material variations, size differences, and geographical factors. Journal of Cleaner Production 2025; 496: 145081. http://dx.doi.org/10.1016/j.jclepro.2025.145081
25. Elduque A, Elduque D, Javierre C, Fernández Á, Santolaria J. Environmental impact analysis of the injection molding process: analysis of the processing of high-density polyethylene parts. Journal of Cleaner Production 2015; 108: 80–9. http://dx.doi.org/10.1016/j.jclepro.2015.07.119
26. Sarma LS, Mallikarachchi C, Herath S. Design-informed generative modeling of skeletal structures using structural optimization. Computers & Structures 2024; 302: 107474. http://dx.doi.org/10.1016/j.compstruc.2024.107474
27. Dong Y, Hussain I, He S. Structural topology optimization of aircraft wing leading edge fabricated of multilayer composites. Aerospace Science and Technology 2025; 159: 109993. http://dx.doi.org/10.1016/j.ast.2025.109993
28. Zheng B. Analysis of Static and Dynamic Characteristics and Lightweight Design of Titanium Alloy Frame. Manufacturing Technology. Jan Evangelista Purkyne University in Usti nad Labem 2024; 24: 507–19. http://dx.doi.org/10.21062/mft.2024.053
29. Chidambaram RK, Pedapati PR, Kanna PR, Taler D, Sobota T, Taler J. Structural assessment of electric two-wheeler battery enclosure: thermal and structural study. Journal of Thermal Analysis and Calorimetry. Springer Science and Business Media LLC 2024. http://dx.doi.org/10.1007/s10973-024-13458-0
30. Prabhuram T, Sundaram SCM, Jegadeeswer S, Kannan VS. Static analysis of different spoke structure of airless and conventional tyre. IOP Conference Series: Materials Science and Engineering. IOP Publishing; 2020; 923: 012017. http://dx.doi.org/10.1088/1757-899x/923/1/012017
31. Bata A, Gerse P, Kun K, Slezák E, Ronkay F. Effect of recycling on the time- and temperature-dependent mechanical properties of PP/MWCNT composite liner materials. Results in Engineering 2025; 25: 104150. http://dx.doi.org/10.1016/j.rineng.2025.104150
32. Dassault Systemes. Simulation, Topology study: SIMP method for topology optimization [Internet]. France: Dassault Systemes; 2025. [cited 2025 Jan 3] Available from: https://help.solidworks.com/2025/spanish/SolidWorks/cworks/c_simp_method_topology.htm?verRedirect=1#